

# Impact of different heating and current drive methods on the early $q$ -profile evolution in JET

**T J J Tala<sup>1</sup>, V V Parail<sup>2</sup>, A Becoulet<sup>3</sup>, C D Challis<sup>2</sup>, G Corrigan<sup>2</sup>,  
N C Hawkes<sup>2</sup>, D J Heading<sup>2</sup>, M J Mantsinen<sup>4</sup>, S Nowak<sup>5</sup> and  
contributors to the EFDA-JET work programme<sup>6</sup>**

<sup>1</sup> Association Euratom-Tekes, VTT Chemical Technology, PO Box 1404, FIN-02044 VTT, Finland

<sup>2</sup> Euratom/UKAEA Fusion Association, Culham Science Centre, Abingdon, Oxon OX14 3DB, UK

<sup>3</sup> Association Euratom-CEA, CEA-Cadarache, F-13108, St. Paul lez Durance, France

<sup>4</sup> Association Euratom-Tekes, Helsinki University of Technology, FIN-02015 TKK, Finland

<sup>5</sup> Association Euratom-ENEA-CNR, Istituto di Fisica del Plasma, Via Bassini 15, 20133, Milano, Italy

Received 19 July 2001

Published

Online at [stacks.iop.org/PPCF/43](http://stacks.iop.org/PPCF/43)

## Abstract

Transport calculations illustrate that the lower hybrid current drive (LHCD) and off-axis electron cyclotron current drive (ECCD) are the only preheating methods that can create a wide, deeply reversed  $q$ -profile, i.e. large negative magnetic shear, on the JET tokamak. Off-axis neutral beam injection (NBI) and off-axis ion cyclotron resonance heating (ICRH) preheating yields a weakly reversed  $q$ -profile (small negative magnetic shear), whereas NBI and ICRH on-axis heating as well as ohmic preheating produce a monotonic  $q$ -profile in the preheating phase. Here, on-axis power deposition and current drive refers to heating and current drive at or close to magnetic axis and correspondingly, off-axis refers to heating and current drive deposited typically around the half minor radius ( $r/a = 0.3$ – $0.6$ ). The results on LHCD, ICRH and ohmic preheating have been verified in the recent JET experiments. The current drive efficiency scan shows that in the case of LHCD, ECCD and off-axis NBI, the driven current is absolutely crucial to obtain a reversed  $q$ -profile and to modify the current profile evolution drastically in the preheating phase. Taking into account only the direct electron heating effect, LHCD does not create a reversed  $q$ -profile. The timing scans indicate that the radial location of  $q_{\min}$  at the end of the preheating phase is generally quite insensitive to the start time of the preheating, once started 0–2 s after the plasma initiation if the method relies upon the driven current. On the other hand, methods relying only upon electron heating are very sensitive to that. In both cases, the magnitude of the negative magnetic shear, however, seems to be very sensitive to the start time of the preheating.

<sup>6</sup> See Pamela J *et al* 2001 Overview of recent JET results and future perspectives *Fusion Energy 2000 (Proc. 18th Int. Conf. Sorrento, 2000)* (Vienna: IAEA) annex.

## 1. Introduction

Tokamak plasma operation with weak or negative magnetic shear and with an internal transport barrier (ITB) is now regarded as the most promising way to increase fusion performance. A hollow current density profile, i.e. a reversed  $q$ -profile (negative magnetic shear), is one of the key conditions that gives rise to the improved core confinement and facilitates the formation of the ITB in advanced tokamak scenarios [1–4].

There are several ways in which magnetic shear  $s$  affects transport, including ITB formation and sustainment. With negative magnetic shear  $s < 0$ , ballooning modes enter the second stable region [5, 6] with complete stability to  $n = \infty$  ideal MHD ballooning modes [7]. The negative magnetic shear also reduces the geodesic curvature drive of micro-instabilities, such as ion temperature gradient (ITG) modes, trapped electron modes (TEMs) and high- $n$  ballooning modes [8] and also reduces magnetic stress [9]. Furthermore, it has also been shown that  $s < 0$  can reverse the toroidal precession drifts of barely trapped electrons [10]. Even some of the high- $k$  turbulences, such as electron temperature gradient (ETG) turbulence, can be stabilized by a region with negative magnetic shear [11, 12]. In the region where  $s \approx 0$ , the turbulent vortices, initially linked together by toroidicity, are more easily disconnected than with large values of  $s$ , thus giving rise to improved plasma confinement. In JET, the effect of the magnetic shear on the evolution of the ITB has been recently analysed in [13].

In order to have the desired  $q$ -profile with all its aforementioned beneficial effects during the high power and plasma performance phase of a tokamak discharge, a successful preparation phase is required to create the appropriate target  $q$ -profile. The preparation phase in the context of this work is called the preheating phase and defined as the time between plasma initiation and the large increase in the heating power (called main heating or high power phase), typically having the heating power 3–10 higher than in the preheating phase. The preheating phase lasts typically 2.5–4.0 s in optimized shear (OS) scenarios in JET. It is also the phase when most of the current ramp up occurs. High plasma current is necessary for good confinement, but current ramp up also plays an important role in establishing the appropriate  $q$ -profile. The purpose of the preheating phase is to bring the plasma to an optimum state for experiments to be conducted at high power phase which further takes advantage of the created  $q$ -profile via the long current diffusion time at high electron temperature in JET. The most important quantity that is to be optimized in the preheating phase is the  $q$ -profile. Other plasma parameters that may be of interest to be modified are pressure and plasma rotation. In addition, avoidance of MHD modes, such as the external kink mode, is also an essential part of the preheating phase as these can cause anomalous current penetration or plasma disruption.

The target  $q$ -profile is defined to be the  $q$ -profile at the end of the preheating phase. In the context of this study, the following definitions for the shapes of the target  $q$ -profiles as illustrated in table 1 are used. In table 1,  $q_0$  denotes the value of  $q$  on the magnetic axis  $R_0$  and  $q_{95}$  is the corresponding value at 95% of the poloidal flux ( $\psi/\psi_{\max} = 0.95$ ).

There are several ways to modify the  $q$ -profile in the preheating phase, i.e. to create the target  $q$ -profile. The method by which to obtain a reversed  $q$ -profile is in principle simple—either to drive off-axis co-current, on-axis counter-current or alternatively to increase the electron temperature in order to slow down the current diffusion from the plasma edge to the

**Table 1.** Definitions for the shape of the  $q$ -profile.

Monotonic $q$ -profile	$q_{\min} = q_0$
Weakly reversed $q$ -profile	$q_{\min} < q_0 < q_{95}$
Deeply reversed $q$ -profile	$q_0 > q_{95}$

centre during the current ramp-up phase. In DIII-D and TFTR, the negative central shear plasmas are formed in the preheating phase with a high power co- or counter neutral beam injection (NBI) together with fast current ramp up [1, 14, 15]. The applicability of electron cyclotron resonance heating (ECRH) and electron cyclotron current drive (ECCD) in the modification of the  $q$ -profile has also been demonstrated in DIII-D [12, 16]. Early neutral beam preheating during the current ramp-up is also used in JT-60U to produce the reversed  $q$ -profile [3, 17]. In the ASDEX Upgrade, the  $q$ -profile is modified in the preheating phase with NBI alone or with a combination of NBI and co- or counter ECCD [4]. In JET, the preheating phase normally consists either of lower hybrid current drive (LHCD) or ion cyclotron resonance heating (ICRH).

Recent JET experiments with motional Stark effect (MSE) measurements show that LHCD preheating can create a deeply reversed  $q$ -profile, while ICRH off-axis preheating creates a weakly reversed  $q$ -profile and a monotonic  $q$ -profile is created by ohmic preheating. Moreover, the recent results on JET also confirm that high performance plasmas with only a moderate heating power can be reached with a reversed  $q$ -profile whereas with a monotonic  $q$ -profile, more power is needed to trigger the ITB and reach the same performance [18]. However, it is still not clear what the optimum target  $q$ -profile should be—deeply reversed, weakly reversed or monotonic. In order to assess and optimize how much off-axis current one can or should drive, which radial location to drive it, and where to deposit the external electron heating power so that the desired target  $q$ -profile could be achieved, detailed modelling of the current density profile evolution is required. The modelling should also test and compare other preheating and current drive methods with those already used in the experiments on JET.

Detailed modelling of the preheating phase, including the comparison of different heating methods during that phase, is lacking at present. Combined kinetic and transport modelling of LHCD and ECCD has been recently analysed in [19]. In this work, complex current profile control scenarios have been studied, concentrating on the predictive modelling of the establishment of the ITB and the control of the ITB with LHCD and ECCD in the main heating phase. The effect of NBI power deposition and current evolution on the ITB formation has been studied in [20]. It was found that, aside from the total input power, the details in power deposition and current density profiles play an essential role in determining the ITB formation threshold power. However, neither of these studies concerned or compared the effect of different heating methods on the  $q$ -profile evolution in the preheating phase.

In the present work, the current profile evolution during the preheating phase in JET has been calculated with the JETTO transport code [21] assuming neoclassical electrical conductivity. The following preheating methods are considered and compared: ohmic, LHCD, on-axis and off-axis ICRH, on-axis and off-axis NBI as well as ECCD. The basic principle used in this study is that the power deposition and external current density profiles are calculated in a self-consistent way. Consequently, the codes to calculate the power deposition profiles are coupled to JETTO to allow a self-consistent simulation cycle between the transport and power deposition (plus current density) calculation with time. This means that all the plasma profiles (such as  $T_e$ ,  $T_i$ ,  $n_e$ ,  $q$ ,  $B_\phi$ ,  $B_\theta$ ,  $I_p$ ,  $Z_{\text{eff}}$  etc) are given as input from JETTO to the heating codes and correspondingly, the heating codes return the power deposition and externally driven current density profiles back to JETTO so that the transport calculation can further proceed. At present there are LHCD, NBI and ECCD modules coupled to JETTO, but no ICRH module has been found that would calculate the power deposition profiles roughly within the same time scale as the transport calculations are performed. Thus, ICRH power deposition profiles are calculated by a separate code.

This paper is organized in the following way. Section 2 introduces the transport model and the modelling of the different heating methods, i.e. the calculation of the power deposition

and current density profiles self-consistently with transport. In section 3, experimental results on the effect of different preheating methods on the  $q$ -profile evolution in the preheating phase are presented. In addition, experimentally measured  $q$ -profiles are compared with the calculated ones. Predictive transport modelling with different preheating methods are analysed in section 4. The preheating methods are compared with each other and current drive efficiency and the effect of varying the duration of the preheating phase are illustrated. The conclusions with a summary are discussed in section 5.

## 2. Modelling of transport and different heating methods

The current density evolution in JETTO transport code [21] is calculated according to the Faraday equation assuming neoclassical electrical conductivity [22]. All the external current sources, such as LH and NB driven current as well as current driven by ECCD, in addition to ohmic and bootstrap current, are taken into account.

The heat transport model is an empirical transport model which is based on a combination of a Bohm and a gyro-Bohm type of anomalous transport. The model has been tested against several different plasma discharges performed on DIII-D, TFTR, JT-60U, ASDEX-U, START and JET in L mode and against many different plasma shots performed on JET in H mode [23–26]. Recently, it has been amended to include an empirical ITB formation threshold condition found in JET [13]. The set of the heat transport coefficients with the ITB threshold condition can be written in the following form:

$$\chi_e = 1.0\chi_{gB} + 2.0\chi_B + \chi_{\text{neo-al}} \quad (1)$$

$$\chi_i = 0.5\chi_{gB} + 4.0\chi_B + \chi_i^{\text{neo}} \quad (2)$$

where

$$\chi_{gB} = 5 \times 10^{-6} \sqrt{T_e} \left| \frac{\nabla T_e}{B_\phi^2} \right| \quad (3)$$

$$\chi_B = \chi_{B_0} \times \Theta(-0.14 + s - 1.47\omega_{E \times B} / \gamma_{\text{ITG}}) \quad (4)$$

with

$$\chi_{B_0} = 4 \times 10^{-5} R \left| \frac{\nabla(n_e T_e)}{n_e B_\phi} \right| q^2 \left( \frac{T_e(0.8\rho_{\text{max}}) - T_e(\rho_{\text{max}})}{T_e(\rho_{\text{max}})} \right) \quad (5)$$

and

$$\chi_{\text{neo-al}} = \frac{c^2 v_{\text{th}}}{\omega_{pe}^2 q R} \epsilon. \quad (6)$$

In (3)–(6),  $T_e$  and  $T_i$  are the electron and the ion temperatures, respectively,  $n_e$  is the electron density,  $B_\phi$  the toroidal magnetic field,  $c$  the speed of light,  $v_{\text{th}}$  and  $\omega_{pe}$  are the electron thermal velocity and plasma frequency and  $R$  is the major radius and  $\epsilon$  the inverse aspect ratio. All the units appearing in (1)–(6) are in SI units except  $T_i$  and  $T_e$  whose units are eV.  $\chi_i^{\text{neo}}$  is the neoclassical term for the ion heat transport [27].  $\chi_{\text{neo-al}}$  represents transport arising from ETG modes and has a similar form that proposed by Ohkawa [28]. Recently, this form of ETG transport has been supported by nonlinear gyrokinetic calculations and was found to match experiments reasonably well [29].

The  $\Theta$ -function multiplying the Bohm transport in (4) is the Heaviside step function with the controlling parameter given by the ITB formation threshold condition found in [13]. When the argument  $x$  in the step function  $x = -0.14 + s - 1.47\omega_{E \times B} / \gamma_{\text{ITG}}$  changes its sign, the ITB

either forms ( $\Theta(x < 0) = 0$ ) or collapses ( $\Theta(x > 0) = 1$ ).  $\omega_{E \times B}$  stands for the flow shearing rate defined as

$$\omega_{E \times B} = \left| \frac{R B_\theta^2}{B_\phi} \frac{\partial}{\partial \Psi} \frac{E_r}{R B_\theta} \right|$$

corresponding to [30] ( $\Psi$  is the poloidal flux,  $E_r$  is the radial electric field and  $B_\theta$  is the poloidal magnetic field) and  $\gamma_{\text{ITG}}$  is the linear growth rate of the ITG instability, defined as  $\gamma_{\text{ITG}} = v_{\text{th},i}/R$  with  $v_{\text{th},i}$  being the ion thermal velocity. Physically, the Bohm-type of anomalous transport  $\chi_B$  (in (1) and (2)) is fully suppressed in regions where the condition  $-0.14 + s - 1.47\omega_{E \times B}/\gamma_{\text{ITG}} \leq 0$  is fulfilled, and the internal transport barrier forms. In the preheating phase, the contribution from the magnetic shear  $s$  is clearly the dominant term in the ITB threshold condition because  $\omega_{E \times B}$  is small with a small input power, especially in the absence of NBI. Recent experiments on JET have also verified that ITBs in the preheating phase are controlled mainly by  $s$ , having an ITB existing roughly in regions where  $s \lesssim 0$ . On the contrary, in the main heating phase there are often two ITBs at the same time, and the outer one is controlled not only by  $s$ , but by the  $\omega_{E \times B}$  shearing rate and rational surfaces of  $q$  [13, 18, 31, 32].

The particle transport is not modelled, but the density is taken from the experiments except in the case of NBI when the density varies with time in the preheating phase and can be much larger than with other preheating methods. Therefore, the amount of externally driven current, like NBI driven current, decreases. The particle diffusion coefficient for the NBI preheated plasmas is defined as  $D \propto \chi_e \chi_i / (\chi_e + \chi_i)$ . The initial and boundary conditions for the ion and electron temperatures as well as the plasma current are taken from the experiment. Also, experimental values for  $Z_{\text{eff}}$  and  $P_{\text{rad}}$  are used.

Toroidal velocity is calculated from the momentum balance equation using the torque from neutral beam injection as the source term. The anomalous toroidal viscosity coefficient is assumed to be equal to the ion heat transport coefficient given in (2). There is experimental evidence on JET, and other tokamaks, that in the NB heated plasmas, the toroidal viscosity coefficient coincides with the ion heat diffusion coefficient, both radially (at least inside  $r/a = 0.8$ ) and as a function of time [33]. However, the contribution from the toroidal rotation is almost negligible in the preheating phase, especially for plasmas without NBI. The poloidal rotation is assumed to be neoclassical.

The most critical assumption in the transport model, especially when investigating the  $q$ -profile evolution during the preheating phase, is the initial  $q$ -profile. Normally no MSE magnetic measurements are available at the beginning or at the time of the preheating phase on JET and consequently, the initial  $q$ -profile must be taken from the EFIT [34] calculation that uses magnetics only. Therefore, in order to reach the maximum accuracy and consistency in the calculation of the  $q$ -profile evolution, the simulations must be started immediately after the plasma initialisation (plasma initialization at  $t \approx 0.5$ , simulation started at  $t \approx 0.5$ – $1.0$  s). As a consequence, the inaccuracy in the  $q$ -profile evolution coming from the initial  $q$ -profile is minimized. In addition, this procedure ensures that the calculated current has the longest time to evolve with neoclassical conductivity in order to reach the maximum consistency with neoclassical theory.

The power deposition and current density profiles of LHCD are calculated with the fast ray tracing code (FRTC) [35]. FRTC includes a fast ray-tracing package and the calculation of the power deposition and current density profiles by iteration between the evaluation of the quasi-linear diffusion coefficient and a one-dimensional (1D) Fokker–Planck equation for the electron distribution function. A comprehensive study of its properties was reported in [36]. FRTC is coupled to JETTO, thus allowing self-consistent simulations between transport

and lower hybrid (LH) power and current calculation. The coupled JETTO/FRTC code was validated in [23].

In order to calculate the NBI power deposition and current density profiles, the NBI code PENCIL [37] is used. PENCIL is also coupled to JETTO. It solves a simplified Fokker–Planck equation that is used to describe the fast ion dynamics. Fast ion self-collisions and the effects of toroidal electric field on the fast ion dynamics are neglected. The resulting bounce averaged Fokker–Planck equation is then solved using an eigenfunction expansion in the pitch angle variable. On-axis/off-axis power deposition profiles are produced by an appropriate selection between the normal and tangential PINIs, normal PINIs producing NBI power perpendicular to the toroidal direction (on-axis power deposition) and tangential PINIs at angles smaller than  $90^\circ$  with respect to the toroidal direction (off-axis power deposition).

The calculation of ECRH and ECCD is done with the three-dimensional (3D) code ECWGB [38]. The code has been recently coupled to JETTO. ECWGB calculates the propagation and absorption of the electron cyclotron waves injected as collimated microwave gaussian beams in toroidal geometry. The ECRH power absorbed and the ECCD current generated by highly collimated gaussian beams are evaluated using the equilibrium from JETTO and the relativistic treatment of the wave propagation and driven current. In addition, the effects of the trapped particles are taken into account. The frequency of the electron cyclotron waves is assumed to be 110 GHz and the poloidal and toroidal angles can be steered to radially change the location of the power absorption and the amount of the generated current.

The only heating method that is not dealt with in a self-consistent way in JETTO is ICRH. The power deposition profiles for electrons and ions are calculated with the ICRH code PION [39]. The PION code calculates ion cyclotron resonance frequency (ICRF) heating power deposition profiles by taking into account the time evolution of the distribution functions of the resonating ions. In the simulations, hydrogen minority scheme (hydrogen concentration typically 2–4%) is applied with frequencies in the range of 42–51 MHz to obtain on-axis and off-axis power deposition. The driven ICRH current has been assessed with the 3D Monte-Carlo code FIDO [40] and was found to be negligible for the chosen ICRH scheme.

### 3. A comparison between the experimental and simulated target $q$ -profiles

Different preheating methods can produce very distinct target  $q$ -profiles. The temporal evolution of the main plasma parameters for three different preheating scenarios in typical JET OS experiments is shown in figure 1. Most of the plasma parameters were the same for all the three discharges, i.e. the toroidal field  $B_\phi$  was 2.58 T, the inductive plasma current was ramped up at about  $0.37 \text{ MA s}^{-1}$  and the average density and  $Z_{\text{eff}}$  were roughly the same. This current ramp rate was applied after an initial fast rise at plasma initialization between  $t = 0.0$ – $1.0$  s. What was distinct between the three pulses was the preheating method; one of them was with LHCD preheating (pulse No 51466), the second one with off-axis ICRF hydrogen minority preheating (pulse No 51470) and the third one with ohmic preheating (pulse No 51456). Consequently, the electron temperatures and current density profiles evolved in different ways. Also shown in figure 1(c) is another LHCD discharge (pulse No 51976) which had similar  $I_p$ ,  $n_e$ , LH power and other plasma parameters, but the toroidal magnetic field was 3.45 T. The preheating phase lasted from  $t = 1.0$  s until  $t = 4.2$  s when diagnostics NBI was added for the MSE measurements.

The target  $q$ -profiles just after the end of the preheating phase at  $t = 4.4$  s for these three different preheating methods are illustrated in figure 2. The  $q$ -profiles have been reconstructed with EFIT equilibrium code using the MSE measurements as the constraints for EFIT [41]. The  $q$ -profiles inside  $R = 3.6$  m are different between the three cases; LHCD and off-axis

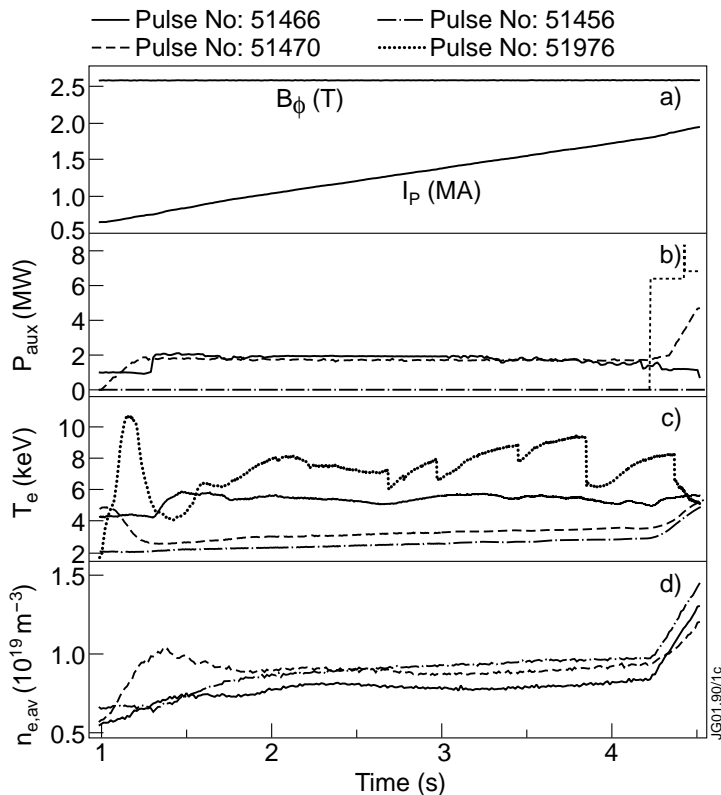


**Figure 1.** (a) Time traces of plasma current and magnetic field; (b) external heating powers; (c) central electron temperatures (electron cyclotron emission measurements) and (d) average electron densities for three discharges with different preheating methods. The full curve refers to the pulse with LHCD preheating; the broken curve with ICRF preheating and the dash-dotted curve with ohmic preheating. The NBI power (short dashed curve in (b)) started at  $t = 4.2$  s is the same for all the three discharges. The dotted curve in (c) is another LHCD preheated pulse with higher  $B_\phi$ .

ICRF preheating created a weakly reversed  $q$ -profile, but with a difference of 10 cm in the radial location of  $q_{min}$  whereas Ohmic preheating produced a monotonic  $q$ -profile. Also shown in figure 2 is the other LHCD preheated discharge with higher magnetic field. This discharge yielded a deeply reversed  $q$ -profile inside  $R = 3.5$  m. The electron temperature data for this discharge (shown in figure 1(c), dotted curve) illustrates the sawtooth-like behaviour often seen in pulses with LHCD preheating. This sawtooth-like behaviour is an experimental indicator on magnetic reconnections which are associated with deeply reversed  $q$ -profiles [31]. This type of target  $q$ -profiles with large negative magnetic shear have been routinely produced with LHCD preheating during the last experimental campaign on JET. Even dozens of discharges with the observation of zero current density in the plasma core region created by LHCD have been recently reported in JET [42].

In order to make a comparison between the  $q$ -profiles reconstructed with EFIT using MSE measurements as constraints and the  $q$ -profile evolution calculated according to neoclassical resistivity, JETTO transport code has been run in an interpretative way. This means that only the Faraday equation for the current density is solved and all the other plasma parameters,

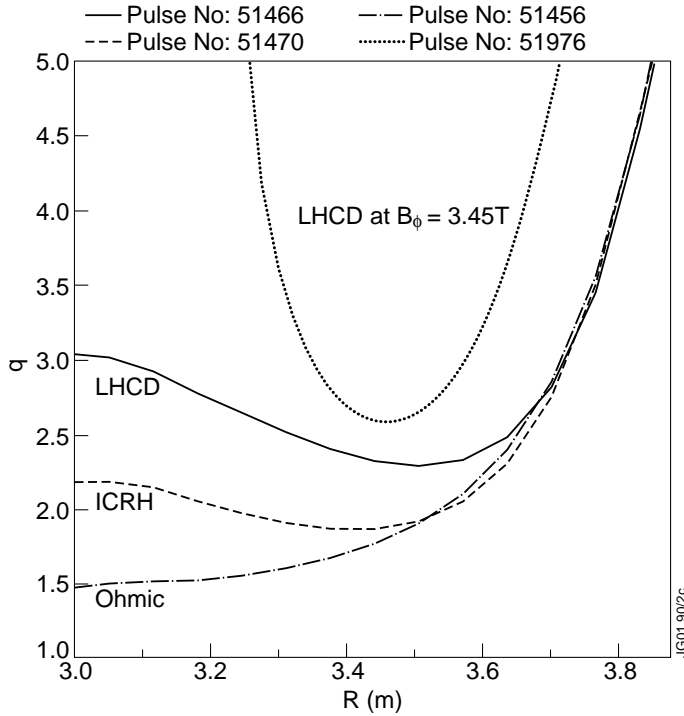


**Figure 2.**  $q$ -profiles at the end of the preheating phase at  $t = 4.4$  s for the different preheating schemes. The full curve corresponds to LHCD preheating, the broken one to ICRF preheating and the dash-dotted one to ohmic preheating. The dotted curve is the other LHCD preheated discharge at higher magnetic field and with a better plasma initialization.

such as temperatures, densities, total plasma current, magnetic field,  $Z_{\text{eff}}$  etc, are taken from the experiments. The simulations are started after plasma initialization at  $t = 1.0$  s.

The result of the comparison just after the end of the preheating phase at  $t = 4.4$  s when the MSE measurements are available is presented in figure 3 for the same preheating method scan discharges as shown in figure 2. The agreement between EFIT and the neoclassical prediction is relatively good in the case of LHCD. The location of  $q_{\text{min}}$  is reproduced accurately within 5 cm which is well within the accuracy of the EFIT+MSE reconstruction and also, the magnetic shear is roughly the same elsewhere except in the core region. Neo-classical resistivity predicts a flat  $q$ -profile (in the limit of a weakly reversed or monotonic  $q$ ) for ICRF preheated discharge whereas EFIT tends to produce a weakly reversed  $q$ -profile. Nevertheless, quantitatively the  $q$ -profiles also seem to be quite similar in the case of ICRF preheating, i.e. the nearly zero shear region is as wide (except the core again) in both cases. In the ohmic preheating, the difference between the electron temperature measurements by Lidar Thomson scattering and electron cyclotron emission (ECE) was significant. As a consequence, the modelling results depend on the  $T_e$  measurements used. The  $q$ -profile calculated with  $T_e$  measurements from ECE (broken curve) are in much better agreement with EFIT outside  $R = 3.3$  m whereas the  $q$ -profile calculated with  $T_e$  measurements from Lidar (dash-dotted curve) is closer to the EFIT one inside  $R = 3.3$  m.

The largest discrepancy between EFIT and neoclassical theory is the core region inside  $R = 3.15$  m, as seen for each preheating method in figure 3. The number of trapped

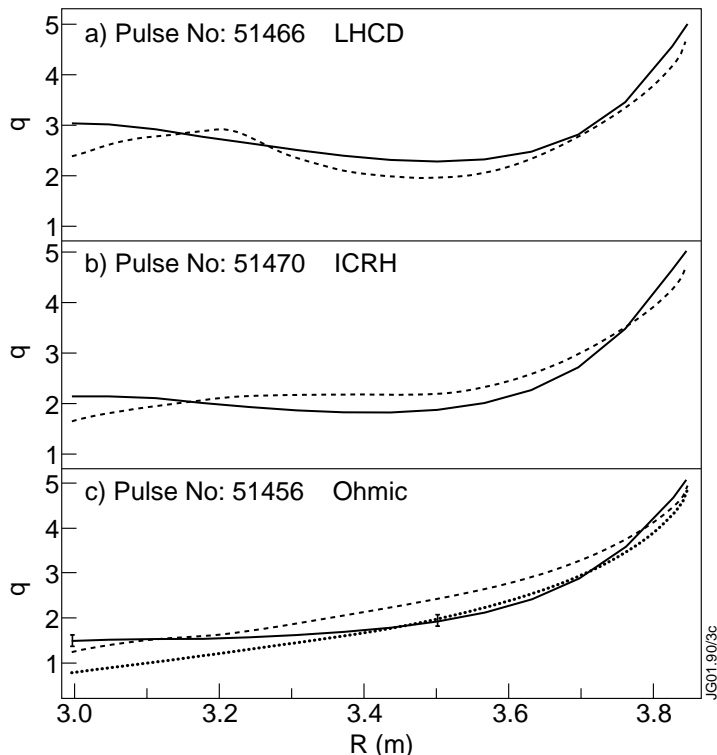


**Figure 3.** EFIT and calculated  $q$ -profiles at the end of the preheating phase at  $t = 4.4$  s for: (a) LHCD; (b) ICRF; and (c) ohmic preheating schemes. The full curves correspond to  $q$ -profiles reconstructed with EFIT and the broken curves are the calculated ones. The dash-dotted curve in (c) is calculated by using Lidar  $T_e$  measurements instead of  $T_e$  from ECE. Also shown in (c) are the estimated error bars at two radii in the reconstruction of the  $q$ -profile with EFIT + MSE.

particles decreases significantly inside this region and thus, because of the increased electrical conductivity, the neoclassical calculations always generate a dip in the  $q$ -profile in the plasma centre. The EFIT solution with prescribed polynomials do not produce this feature. When the classical Spitzer conductivity instead of the neoclassical one is assumed, the agreement between the  $q$ -profiles calculated with EFIT and JETTO is not as good. The magnitude of the Spitzer conductivity is a factor of 2–3 larger than the neoclassical one and consequently, it tends to create far too large values for  $q$  inside  $R = 3.6$  m although it does not create the dip in the  $q$ -profile as the neoclassical conductivity does. The earlier experimental results on JET have also demonstrated that neoclassical conductivity is more consistent with experiments than the Spitzer conductivity [43].

The neoclassical conductivity calculated by JETTO is in a very good agreement with the conductivity calculated by a neoclassical transport code NCLASS [44]. The difference in the conductivity is about 2–4% between JETTO and NCLASS, which treats the neoclassical theory in a more sophisticated way and with fewer simplifying approximations than JETTO [21]. Moreover, the comparison of results from the two codes indicates that the difference in the magnitude of the bootstrap current is within 5% outside  $R = 3.15$  m and inside that radius it is of the order of 5–20%. The largest difference is found in the cases with a deeply reversed  $q$  where the value of  $q$  in the centre exceeds 20.

In general, the largest uncertainties in the neoclassical JETTO calculations of the  $q$ -profile evolution are the initial  $q$ -profile problem already discussed in section 2 and the electron temperature measurements. The initial  $q$  from EFIT with magnetics only at  $t = 1.0$  s was in each three cases shown in figure 3 very monotonic (large positive magnetic shear). By using a flat initial  $q$ -profile instead of the EFIT one, target  $q$ -profiles at  $t = 4.4$  s slightly closer to EFIT + MSE profiles in the case of ICRH and ohmic preheating can be obtained with JETTO. The other source of error are the electron temperature measurements which determine the neoclassical conductivity. The error in  $T_e$  measurements is typically of the order 10–20% in the early preheating phase of the plasma discharge and in some cases the difference between Lidar and ECE is significant, as was the case in the discharge with ohmic preheating as shown in figure 3.

#### 4. Effects of different preheating methods on $q$ -profile evolution

A comparison of the electron temperature profiles between the experiments and predictive JETTO calculations during the preheating phase is presented in figure 4. The three discharges (Pulses No 51456, 51466 and 51470) are the same ones as already presented in figures 1, 2 and 3. The start time of the simulations is at  $t = 1.0$  s. The agreement between the measured and calculated  $T_e$  profiles is well within the accuracy of the measurements of  $T_e$  ( $\approx 20\%$ ) for all heating methods and at any time during the preheating phase. The difference between the experiment and the simulation tends to be slightly larger in the case of LHCD. This is presumably due to the larger inaccuracies in the modelling of LH power deposition and current density profiles than in the modelling of ICRF power deposition or simulations without any external heating as in the ohmic case.

##### 4.1. ICRF preheating

In hydrogen minority ICRF preheating, the time evolution of  $T_e$  and  $q$  depends on the location of the ion cyclotron resonance. The power deposition, electron temperature and  $q$ -profiles for three different resonance locations are illustrated in figure 5. All the basic plasma parameters as well as the initial and boundary conditions for  $T_e$  are taken from the pulse No 51897, which has a preheating phase similar to 51976. The simulations start at  $t = 1.0$  s. 5 MW of on-axis ICRF preheating creates a monotonic target  $q$ -profile (although  $s$  is close to zero) whereas different off-axis power deposition profiles produce a weakly reversed target  $q$ -profile if the heating starts immediately after the plasma initialization. Otherwise, if the start of the heating is delayed by more than 1 s, a reversed  $q$ -profile is not achieved. The same conclusion on ICRF preheating could be drawn from the  $q$ -profiles reconstructed with EFIT using MSE measurements as constraints in section 3.  $q_{\min}$  is located at the peak of the power deposition, however not outside  $R = 3.35$  m. With the hydrogen minority heating scheme, about 80% of the ICRH power (5 MW) goes to electrons. Modelling indicates that in order to create a deeply reversed  $q$ -profile with ICRF preheating, either the power deposition profile should be narrower or the slowing down time of the fast ions colliding with the electrons should be shorter (both options are difficult in practice).

##### 4.2. LHCD preheating

In order to separate the effects of the electron heating and the current drive on the  $q$ -profile evolution in the case of LHCD preheating, an LH current drive efficiency scan is performed. The LH driven current calculated by FRTC is multiplied throughout the simulations either

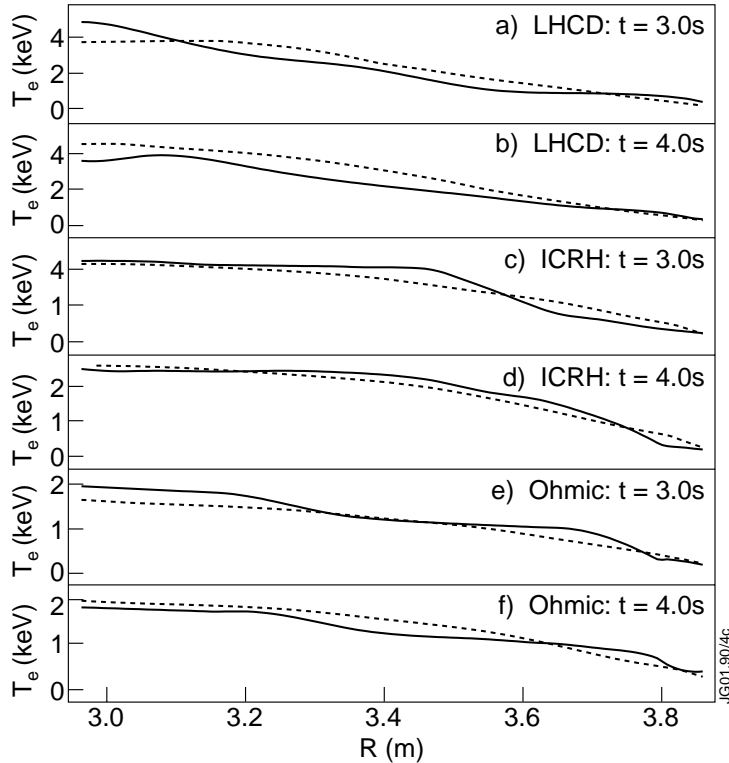


**Figure 4.**  $T_e$  profiles at  $t = 3.0$  s and at  $t = 4.0$  s for: (a) and (b) LHCD; (c) and (d) ICRF; and (e) and (f) ohmic preheating schemes. The full curves correspond to the measured  $T_e$  profiles and the broken curves are the calculated ones.

by 1.0, 0.5, 0.25 or 0.0 with 1.0 corresponding to the actual current evaluated by the ray-tracing code and 0.0 corresponding to the case with the LH heating only. All the basic plasma parameters as well as the initial and boundary conditions for  $T_e$  are taken again from the pulse No 51897. LH power is 3 MW and the driven LH current 400–800 kA (depends on time) in the case with the actual LH current calculated by FRTC (multiplication by 1.0). In the other cases the driven LH current decreases roughly with the multiplication factor. The simulations start at  $t = 1.0$  s, and the modelling results of the main profiles at the end of the preheating phase at  $t = 5.0$  s are presented in figure 6.

The LH current efficiency scan shows that the driven current seems to be absolutely crucial in order to create a reversed  $q$ -profile. As shown in figure 6, the  $q$ -profile is monotonic if the LH driven current is fully neglected (dotted curve). However, taking into account only 25% of the calculated LH current (dash-dotted curve) seems to be enough to reverse the  $q$ -profile. Moreover, the experimental results provide an additional, although indirect, verification of the importance of the LH driven current. If the power deposition profiles of LH (in figure 6(b), full or broken curves) and hydrogen minority off-axis ICRH (in figure 5(a), broken or dash-dotted curves) are compared, they can be regarded as being qualitatively similar during the preheating phase on JET, i.e. the power deposition profiles are very wide and are deposited mostly at radii  $r/a \approx 3.1$ – $3.5$  m. Consequently, having assumed a negligible contribution from the LH driven current, the  $q$ -profile evolution should be fairly similar in plasmas with LH and ICRF preheating at the same power level. However, the experimental results, such

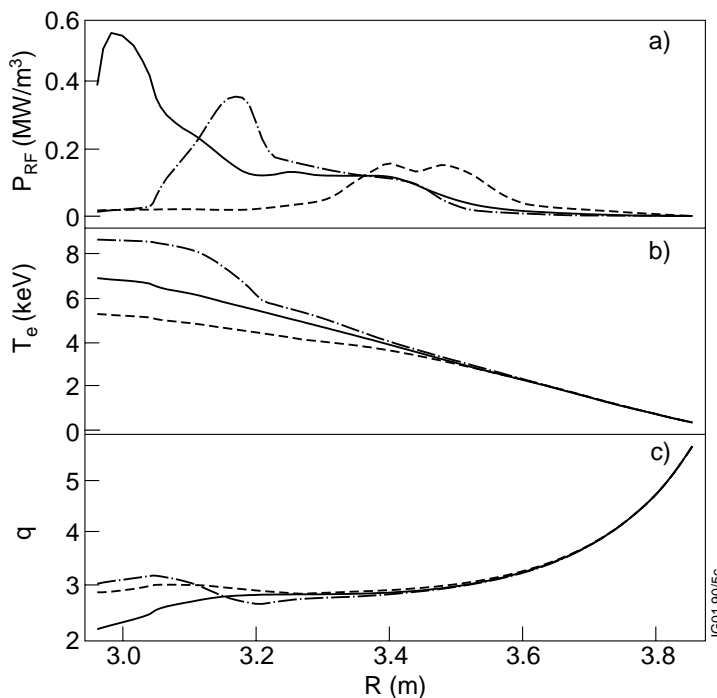


**Figure 5.** (a) The power deposition profiles (to electrons); (b)  $T_e$  profiles; and (c) the target  $q$ -profiles for the three different locations of the ion cyclotron resonance at the end of the preheating phase at  $t = 5.0$  s.

as shown for example in figure 2, indicate significantly different target  $q$ -profiles at the end of the preheating phase; a deeply or weakly reversed  $q$  with LHCD and a weakly reversed  $q$  with ICRH. To sum up, both the LH current drive efficiency scan and the distinct experimental behaviour of the  $q$ -profile with LHCD and off-axis ICRF preheating emphasize the significance of the role of the LH driven current in the modification of the  $q$ -profile.

### 4.3. NBI preheating

The role of particle transport becomes more important in the case of NBI preheating since the external current drive is inversely proportional to density. Furthermore, additional gas puffing must be used in order to avoid excessive shine through of the beams due to too low density. The simulation results of NBI preheating are shown in figure 7. Again, the plasma parameters from the pulse No 51897 are used, but now particle transport is also modelled and gas puffing used in order to exceed the minimum density limit for NBI system to operate safely. The input power is 5 MW and the driven NBI current is of the order of 130–180 kA both with on-axis and off-axis cases.

As seen in figure 7, 5 MW of NBI on-axis preheating creates a monotonic  $q$ -profile whereas 5 MW of NBI power deposited off-axis weakly reverses the target  $q$ -profile. Similarly to LHCD, without taking into account the externally driven NB off-axis current (dash-dotted curve), a reversed target  $q$ -profile cannot be achieved. In the case of off-axis NBI, the  $q$ -profile is more strongly reversed between  $t = 2.0$  s and  $t = 4.0$  s, but after  $t = 4.0$  s the rising density decreases the NB driven off-axis current and consequently, plasma current starts to

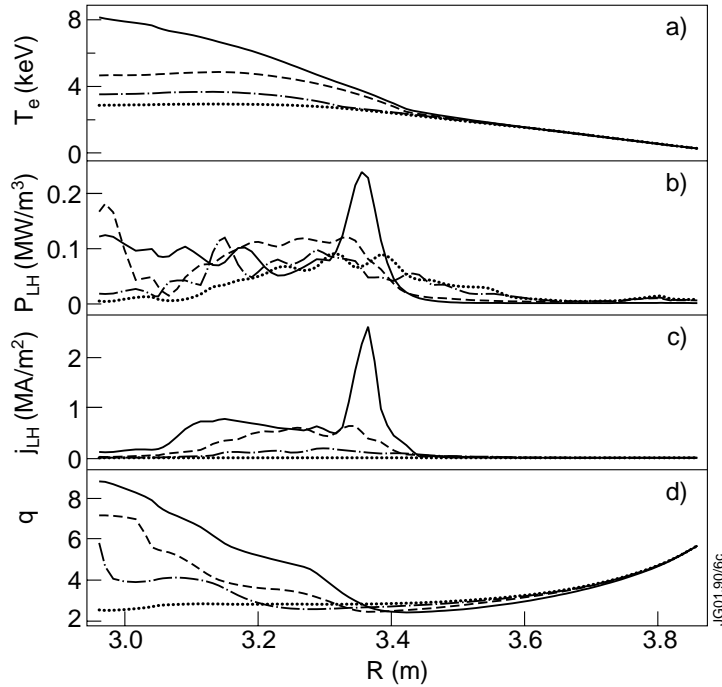


**Figure 6.** (a) Electron temperature; (b) LH power deposition profiles; (c) LH driven current; and (d) the target  $q$ -profiles at  $t = 5.0$  s. The calculated LH current is multiplied either by 1.0 (full curves), 0.5 (broken curves), 0.25 (dash-dotted curves) or by 0.0 (dotted curves).

accumulate in the plasma centre. The off-axis power deposition profile shown in figure 7(a) (broken curve) is the most off-axis power deposition profile that is achievable with the present JET NBI system (only tangential beams are used). Therefore, the maximum radius for  $q_{\min}$  with NBI preheating is  $R = 3.35$  m. Since the density is low in the preheating phase, the shine-through effect decreases the launched power by 15–20%, and additionally, only 45–55% of the absorbed power goes to electrons. Accordingly, the effective heating power that goes to electrons is less than half of the launched NBI power.

In order to complete the analysis of the NBI preheating, counter on-axis NBI preheating is also studied. The simulation results show that at the early phase of the preheating phase ( $t \approx 2$  s), the  $q$ -profile is deeply reversed, but the radius of  $q_{\min}$  is quite small ( $R = 3.2$  m). In the early phase the NB driven negative on-axis current is about  $-300$  kA. However, after 2 s the NB current drive efficiency starts to decrease due to increasing density and  $q$  becomes less reversed and finally after  $t = 4$  s  $q$  becomes monotonic.

#### 4.4. ECCD preheating

In ECCD preheating, the location of the power deposition and current density profiles is determined mainly by the frequency of the electron cyclotron waves and the magnetic field in the plasma, which are both fixed quantities and usually do not vary much during the experiment. On the other hand, the amount of absorbed power of the total launched power and the amount of the driven current depend strongly on the electron temperature and density. The absorbed power increases with increasing  $T_e$  and  $n_e$  whereas the driven ECCD current increases with increasing

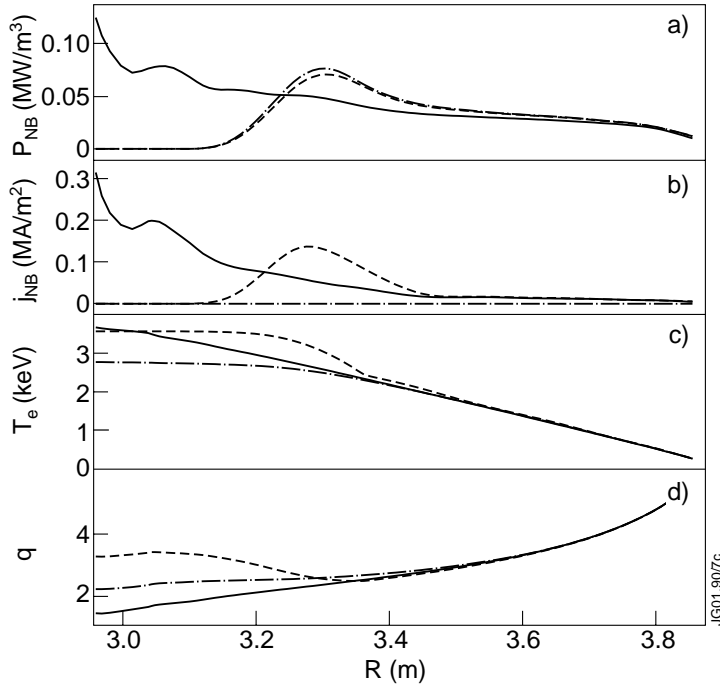


**Figure 7.** (a) Power deposition profiles (to electrons); (b) NB driven current density profiles; (c)  $T_e$  profiles; and (d) the target  $q$ -profiles for on-axis (full curve) and off-axis (broken curve) NBI preheating scenarios at  $t = 5.0$  s. The dashed-dotted curve is the same off-axis scenario, but neglecting the NB driven current.

$T_e$ , but decreases with increasing  $n_e$ .  $Z_{\text{eff}}$  can also vary significantly in the preheating phase and increasing  $Z_{\text{eff}}$  decreases ECCD efficiency. These well known dependences are much more pronounced in the preheating phase where the density is typically very low (of the order of  $1 \times 10^{19} \text{ m}^{-3}$ ) and the electron temperature varies from 2 keV up to 15 keV.

Three different off-axis ECCD preheating scenarios are compared in figure 8. Similarly to other preheating methods, the plasma parameters are taken from pulse No 51897 and the input power is 5 MW. Different locations of the ECCD power deposition profiles are obtained by changing the poloidal angle of the launched waves. The toroidal angle is fixed at  $15^\circ$  with respect to the perpendicular direction. The difference between the electron temperatures in (c) and (d) and correspondingly between  $q$ -profiles in (e) and (f) is a consequence of the used transport model. In (c) and (e), the transport model is the same as presented in section 2 and used everywhere in this paper, but in (d) and (f), the option of having reduced transport, i.e. an ITB when  $s < 0$  is ignored ( $\Theta(x) = 1$  all the time). As already discussed in section 2, there is a lot of experimental evidence to assume reduced transport when  $s \lesssim 0$  in the preheating phase and thus, the reason for using the different transport model is to test the sensitivity of the  $q$ -profile evolution to the applied transport model.

As shown in figure 8(e), deeply or weakly reversed target  $q$ -profiles are achieved with ECCD preheating, depending on the radial location of the peak in the power deposition profile.  $q_{\text{min}}$  is located at the same radius as the peak in the power deposition profile. A weakly reversed target  $q$  with the radius of  $q_{\text{min}}$  as far as  $R = 3.6$  m can be produced with ECCD. If no reduced transport is assumed, the electron temperatures are smaller (in (d)), but the  $q$ -profiles are

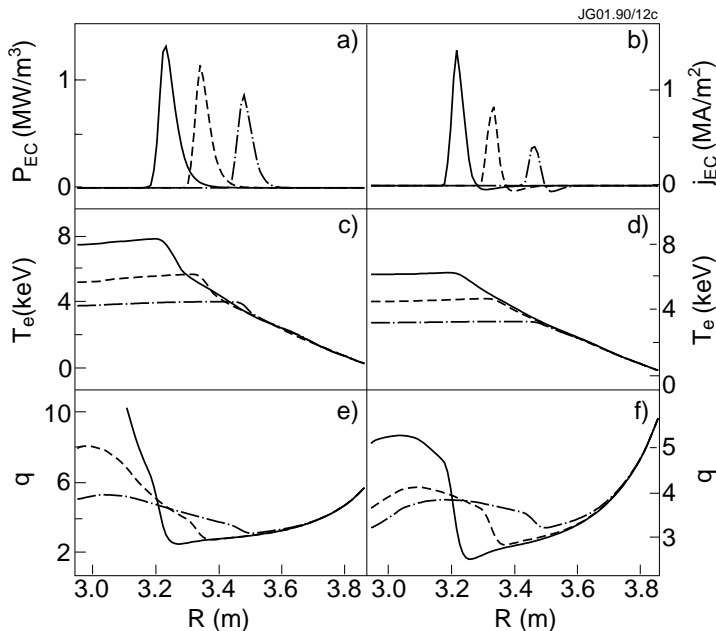


**Figure 8.** (a) ECCD power deposition profiles; (b) ECCD driven current density profiles; (c)  $T_e$  profiles with standard transport model; (d)  $T_e$  profiles with modified transport model; (e) the target  $q$ -profiles with standard transport model; and (f) the target  $q$ -profiles with modified transport model for three different off-axis ECCD preheating scenarios at  $t = 5.0$  s.

still weakly reversed (shown in figure 8(f)), however not deeply reversed any longer as with ITBs in figure 8(e). This indicates that the calculated  $q$ -profile evolution is sensitive to the transport model, but on the other hand, the results with using the very conservative estimate for electron heat transport (no ITB model) also indicate that ECCD is a very efficient tool to modify the  $q$ -profile evolution in the preheating phase. It is also worth noting the difference in the  $q$ -profiles in the core between figures (e) and (f); in (e)  $s$  is negative everywhere inside  $q_{\min}$  whereas in (f)  $s$  is only locally negative around the peak of the ECCD power deposition profile. Another point worth mentioning is the amount of absorbed power and driven ECCD current. In the innermost case (full curves), almost full power absorption is reached (98%), but in the middle one (dashed curves) only about 94% is absorbed and in the outermost case only 90% of the launched power is absorbed in the plasma. The corresponding figures of merit for the driven ECCD current are 160 kA, 120 kA and 70 kA, respectively. Still, this amount of the driven ECCD current plays an important role in the evolution of the  $q$ -profile in the preheating phase. Using ECRH (heating only, toroidal launching angle zero) does not create a deeply reversed target  $q$ -profile with any location of the power deposition profile (weakly reversed target  $q$ -profiles are still possible).

It is not possible to apply on-axis ECCD for all  $B_\phi$  at a fixed frequency (110 GHz) of the electron cyclotron waves. In order to assess the ability of the counter on-axis ECCD to modify the  $q$ -profile evolution in the preheating phase, a similar preheating phase but with a toroidal magnetic field  $B_\phi = 3.7$  T is used. A deeply reversed  $q$ -profile can be achieved with counter on-axis ECCD, however, the region of the negative shear is clearly narrower than in most of the off-axis cases, as being located always inside  $R = 3.3$  m. The ECCD driven current is much larger than in the off-axis cases, reaching nearly  $-300$  kA. Moreover, the calculation indicates

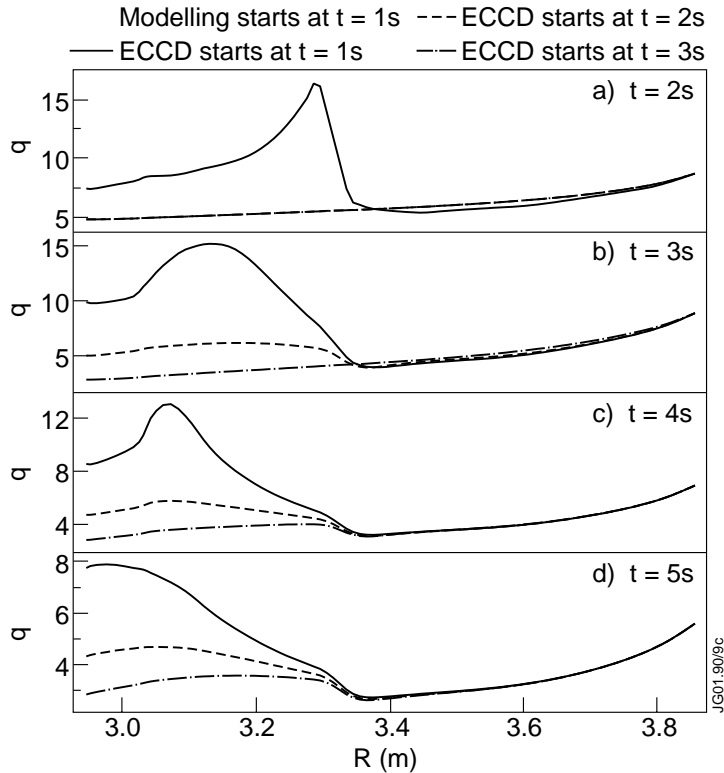


**Figure 9.** (a)  $q$ -profiles at  $t = 2.0$  s; (b) at  $t = 3.0$  s; (c) at  $t = 4.0$  s; and (d) at  $t = 5.0$  s for three different instants when ECCD preheating is switched on. ECCD starts either at  $t = 1.0$  s (full curve), at  $t = 2.0$  s (broken curve) or at  $t = 3.0$  s (dash-dotted curve).

that the central electron temperature can reach 20 keV, by far higher than ever achieved on JET.

The effect of the start time of the ECCD preheating is investigated in figure 9. As can be seen, it plays a major role. Delaying ECCD by 1 s does not produce a deeply reversed target  $q$ -profile and delaying it by 2 s creates almost a monotonic  $q$ -profile. Nevertheless, the location of  $q_{\min}$  remains almost unchanged. Other preheating methods give similar timing scan results; the deepness of the reversed  $q$  is very sensitive to the start time of the preheating whereas the location of  $q_{\min}$ , if it still exists, does not vary much.

#### 4.5. Comparison of different preheating methods

The target  $q$ -profiles at  $t = 4.0$  s and  $t = 5.0$  s produced by the different preheating methods are compared in figure 10. In the simulations, the main plasma parameters and the initial and boundary conditions for  $T_e$  are taken from the pulse No 51897. The external heating power is 5 MW except in the case of LHCD when the power is 3 MW. Thus, the simulations are identical except in terms of the heating and current drive methods.

The preheating methods can be divided into three categories in terms of the created target  $q$ -profile. LHCD and ECCD form category 1 as being the only methods which can produce deeply reversed  $q$ -profiles. Quantitatively the  $q$ -profiles produced by LHCD and ECCD look quite similar. However, the central values of  $q$  are distinct. With LHCD,  $q$  tends to increase

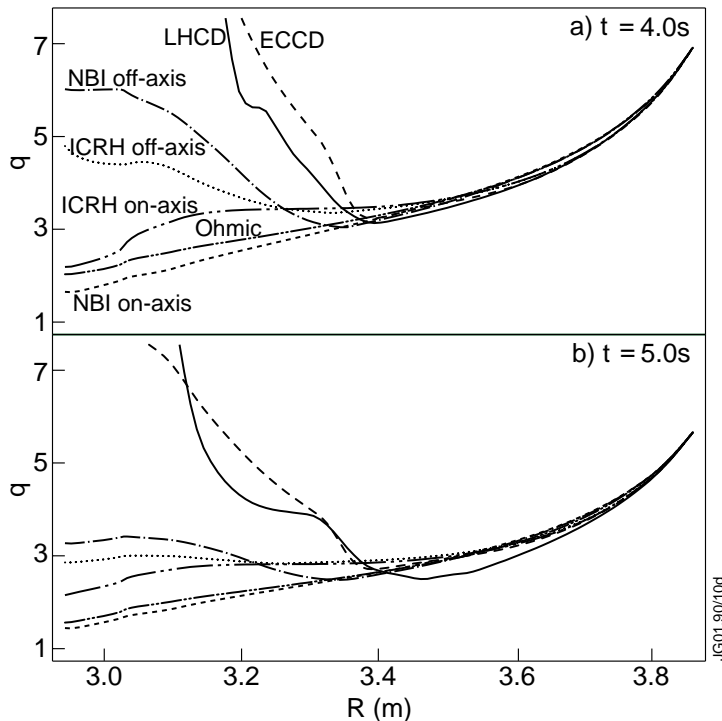


**Figure 10.** (a) Target  $q$ -profiles produced with different preheating methods at  $t = 4.0$  s; and (b) at  $t = 5.0$  s. Category 1, LHCD (full curve) and ECCD (broken curve); category 2, off-axis NBI (dash-dotted curve) and off-axis ICRH (dotted curve); category 3, on-axis NBI (short dashed curve), on-axis ICRH (long double dot-dashed curve) and ohmic (short double dot-dashed curve).

to very high values, such as  $q_0 \approx 30$ – $50$  whereas in the case of ECCD,  $q_0$  remains between 10 and 20. This difference arises mainly from the amount of driven off-axis current; LHCD driven current is of the order of 500–900 kA whereas ECCD current is only 70–160 kA. Large off-axis current can transiently drive the total current density in the core to zero, as has been recently observed in JET [42]. Category 2 consists of off-axis NBI and off-axis ICRH heating which create weakly reversed  $q$ -profiles with  $q_{\min}$  located inside  $R = 3.4$  m. On-axis NBI, on-axis ICRH and ohmic preheating belong to category 3 as they can only create monotonic target  $q$ -profiles.

In the simulations shown in figure 10, the initial  $q$ -profile was taken from EFIT without MSE measurements, the latter being never available at  $t = 1.0$  s. EFIT always gives either a flat or monotonic  $q$ -profile; for pulse No 51897 it turned out to be flat. Therefore, in order to test the sensitivity of the target  $q$ -profiles at  $t = 4.0$  s or  $t = 5.0$  s to the initial  $q$ , the same simulations, as illustrated figure 10, with reversed and monotonic initial  $q$ -profiles were performed. The methods in categories 1 and 3 turned out to be insensitive to the initial  $q$ , giving similar results as shown in figure 10 independently of the initial  $q$ -profile. However, the methods in category 2 tended to give more reversed target  $q$ -profiles in the case of a reversed initial  $q$  and flatter or monotonic  $q$ -profiles in the case of a monotonic initial  $q$ . As a consequence, the simulation results of the preheating methods in category 1 and 3 can be regarded as robust results as being almost independent of the initial  $q$ -profile whereas somewhat larger uncertainties in the results with the methods in category 2 remain. Variations within the accuracy of the measurements in the initial  $T_e$  do not affect significantly the target  $q$ -profile.

The sensitivity of the  $q$ -profile evolution to the uncertainties in the power deposition profiles is an important issue. In the case of NBI and ICRH, the sensitivity can be indirectly inferred by comparing the  $q$ -profiles calculated with on-axis and different off-axis power deposition profiles shown in figures 5(a) and 7(a). As can be seen from the relatively small difference in the target  $q$ -profiles between the two extreme cases (on-axis versus off-axis) in figures 5(c) and 7(c), the  $q$ -profile evolution cannot be very sensitive to small uncertainties coming from the modelling of the power deposition profiles with PION and PENCIL. In the case of LHCD, artificially shifting the power deposition profile either by 10 cm outwards or inwards does not have a significant effect on the target  $q$ -profile at  $t = 5.0$  s. On the other hand, as already shown in figure 6, the  $q$ -profile evolution is very sensitive to the magnitude of the LH driven current. However, assuming only a 50% accuracy in the magnitude of the LH driven current changes neither the location of  $q_{\min}$  nor qualitatively the shape of the target  $q$ -profile very much, as shown in figure 6(d). Quantitatively the changes are within 30% as shown in figure 6(d) as the difference between the full and broken curves. Besides, the assumption of only 50% accuracy in the ray-tracing calculation of the LH driven current with FRTC can be regarded as a very conservative estimation. Ray tracing in the frequency range of the electron cyclotron waves is generally regarded as a robust and reliable method. Consequently, no large uncertainties arising from the modelling of ECCD are expected.

One could argue why the preheating phase is so long, typically being from  $t = 1.0$  s until  $t = 3.5$ – $5.0$  s. The main reason is that, for example, at  $t = 2.5$  s the total plasma current is only about 1.2 MA and as a consequence, the values of  $q$ , even  $q_{\min}$  are well above three. As already discussed in section 2, there is strong evidence that the integer surfaces of  $q$  (especially  $q = 3.0$ ,  $q = 2.0$  and  $q = 1.0$ ) play a key role in triggering the outer ITB in the main heating phase [31, 32, 45]. Thus, starting the main heating too early at  $t = 2$ – $3$  s would yield a longer period of full heating without ITB which generally is not desirable. In addition, at  $t = 2$  s or  $t = 3$  s the  $q$ -profile is still evolving strongly due to the external heating and current drive and the shape of the  $q$  is not necessarily the desired one.

The power deposition profiles (electron channel) and the electron temperature profiles for the same preheating method scan, as shown in figure 10, are compared in figure 11. The very localized nature of the ECCD power deposition profile can be easily seen as the highest peak among the power deposition profiles from the different preheating methods. The two separate peaks in the LHCD power deposition profiles are from the different absorption mechanisms in the single pass and multi pass regimes of lower hybrid waves. NBI preheating and ohmic preheating produce clearly smaller electron temperatures than the other methods. With equal heating power, LHCD would create significantly higher  $T_e$  compared with the other ones.

## 5. Summary and conclusions

The preheating phase in JET has been studied in a very detailed way. The main emphasis was to modify the  $q$ -profile evolution in the preheating phase. JETTO transport code was used to model the current diffusion and heat transport. Separate codes to calculate the power deposition and current density profiles of LHCD, ECCD and NBI have been coupled to JETTO to allow a self-consistent calculation cycle between transport and heating and current drive evaluation. Different preheating methods were compared and the role of externally driven current versus direct electron heating in the  $q$ -profile evolution was discussed.

The different preheating methods could be divided into three categories in terms of the produced target  $q$ -profiles. LHCD and ECCD formed category 1 since they were the only methods which created deeply reversed target  $q$ -profiles in JET. Category 2 consisted of off-axis NBI and off-axis ICRH preheating which produced weakly reversed  $q$ -profiles with  $q_{\min}$

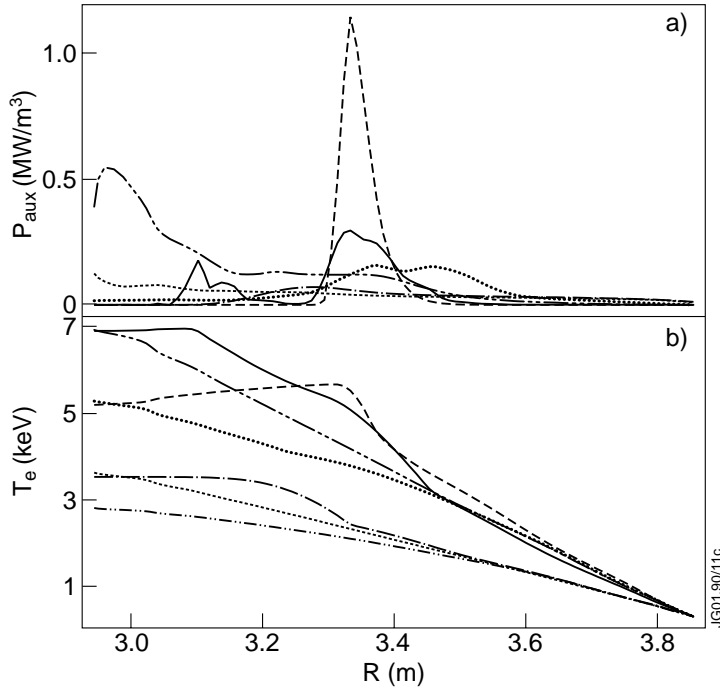


**Figure 11.** (a) Power deposition profiles (electron channel); and (b) electron temperature profiles at  $t = 5.0$  s for the same cases as shown in figure 10.

located inside  $R = 3.4$  m. On-axis NBI and on-axis ICRH and ohmic preheating belonged to category 3 as they created only monotonic target  $q$ -profiles. Experimental results on LHCD, ICRH and ohmic preheating on JET verified the predictive modelling results.

The current driven by LHCD and ECCD was found to be a crucial factor in producing deeply reversed target  $q$ -profiles in the preheating phase. Also, the NBI driven current turned out to be very important in the off-axis NBI preheating scheme. Other important factors affecting the  $q$ -profile evolution in the preheating phase were found to be the width of the power deposition profile and the start time of the preheating with respect to plasma initialization. A narrow off-axis power deposition profile was able to slow down the ohmic current diffusing from the plasma periphery to the centre much more efficiently than a wide one. Moreover, the earlier was the preheating started, the more was the current diffusion slowed down. Since ICRF preheating has wider power deposition profiles than ECRH and it also has an additional slowing down time of the fast ions colliding with the electrons ( $\approx 0.5$  s in JET) that is missing in the ECRH scheme, it is understandable that ECRH preheating (even without any ECCD current) turned out to be a more efficient tool with which to modify the  $q$ -profile evolution in the preheating phase than ICRH.

How well the desired target  $q$ -profile can be sustained later in the main heating phase depends on the applied heating and current methods and the power levels. Bootstrap current and its alignment with the external current drive becomes an important issue. Recent experimental results on the  $q$ -profile evolution in the main heating phase on JET can be found in references [18, 41, 46–48]. Detailed modelling of the  $q$ -profile evolution and a comparison between different heating methods in the main heating phase is beyond the scope of this paper and it is left for future publications although it is known to be a key issue in order to be able to

understand better the physics of the ‘advanced’ tokamak scenarios. Furthermore, in the main heating phase hybrid effects of two or more heating methods can provide excellent tools with which to modify and control the  $q$ -profile evolution. One example is a combination of LHCD with off-axis ECCD where the local off-axis increase in the electron temperature could control the damping of LH waves and thus the location of a large amount of the driven LH current. ECCD efficiency may also improve in the presence of an LH tail due to fast electrons. The combination of LHCD and ECCD has been recently modelled in [19]. Other very interesting hybrid effects to sustain the achieved target  $q$ -profile in the main heating phase would be a combination of LHCD with some on-axis counter current drive method, such as counter NBI, counter ECCD or counter fast wave current drive (FWCD).

There is one serious issue in the modelling that has not been touched in this paper. It is the sawtooth-like behaviour shown in  $T_e$  in figure 1. It is associated with the negative magnetic shear in the core region and the reason for these events are believed to be the neoclassical or double tearing modes [50] or the resistive interchange modes [51]. Similar oscillations have been also observed on Alcator C-Mod [51]. The possible redistribution of the current has not been taken into account in the modelling of the  $q$ -profile evolution. This sawtooth-like behaviour does not lead to a full redistribution of the current which could be modelled and for the present, there is no model in JETTO for the possible partial current redistribution caused by these events.

It is not yet known what the optimum target  $q$ -profile is. Naturally it depends on what the aim of the experiment is, but some general rules can be drawn. The optimum target  $q$ -profile should provide the largest sustainable improvement in the fusion performance while it should also provide MHD stable plasma and good confinement. It should be also sustainable in the main heating phase by non-inductive current drive aligned well with bootstrap current (pressure gradient). Moreover, it should assist the ITB to form as wide as possible in  $r/a$  (broad  $T_i$ ,  $T_e$  and  $n_e$  profiles) and with moderate gradients. This implies that  $q_{\min}$  should be also located as far off-axis as possible and preferably also having an integer value of  $q$  ( $q = 2$  or  $q = 3$ ) close to it, as has been reported in [31, 32, 45].

Each shape of the  $q$ -profile, deeply reversed, weakly reversed and monotonic  $q$ , has advantages and disadvantages with respect to plasma performance, MHD stability, confinement and steady-state operation. The advantages of a deeply reversed  $q$ -profile are a low power threshold to form an ITB at a wide radius [18] and a reduction of various types of turbulence, such as ETG and TEM as discussed in detail in section 1. The disadvantage is that the steady-state is not reached before the performance is lost presumably due to global pressure driven modes or some MHD activity near low-order rational surfaces of  $q$  in the core region [18]. In addition, impurity accumulation in the plasma core seems to be a serious issue with a deeply reversed  $q$ -profile with peaked density profiles [49]. The advantages of the operation with a weakly reversed  $q$  are the absence of low-order rational  $q$ -surfaces in the core and thus the disconnection of turbulent vortices linked together with toroidicity. Higher power threshold to obtain improved performance and the absence of some turbulence stabilizing mechanisms that are based on the large negative magnetic shear can be listed as drawbacks with a weakly reversed  $q$ . With monotonic  $q$ , the advantage is that it can be presumably sustained (remain frozen) most easily in the very long steady-state plasmas. However, the power threshold to form an ITB is clearly the highest among these cases and the stability with respect to many branches of turbulence (TEM, ETG, etc) is the poorest. The future experiments and modelling should be directed towards further understanding of the link between the  $q$ -profile and the performance, the evolution of the ITBs, confinement, MHD stability as well as turbulence suppression.

The experimental results on the  $q$ -profile evolution on other tokamaks in the preheating phase are not identical to the present modelling results. On DIII-D, JT-60U and ASDEX-U,

NBI on-axis preheating is used as the standard method to obtain a reversed  $q$ -profile whereas the present calculations showed that the reversed target  $q$ -profile cannot be created in JET (except transiently for a period of less than 1 s immediately after switching on NBI heating). This is due to the larger volume and the larger major radius on JET than on the other tokamaks; the power density is much smaller and the relative radius that is covered by NBI preheating is also smaller in JET. The same difficulty concerns basically all the methods based on on-axis heating and current drive in JET. On the other hand, the long current diffusion time because of the large major radius allows the off-axis methods to work efficiently on JET if either the power deposition profile is narrow or the driven current large.

The importance of the preheating phase in the preparation of the plasma in ‘advanced’ tokamak scenarios in order to improve fusion performance is obvious in JET. Due to the long current diffusion time, optimizing the  $q$ -profile in the preheating phase gives rise to enhanced performance in the high power phase by improving both confinement and MHD stability as well as obtaining a large fraction of well-aligned bootstrap current. In ITER, the current diffusion time is huge during the burn phase. Therefore, in order to improve and optimize fusion performance in ITER, very careful plasma preparation, especially optimizing the  $q$ -profile is required. As a consequence, preheating techniques and analyses similar to that presented in this paper should be considered for ITER in future.

## Acknowledgments

The authors like to thank Wayne Houlberg for his great efforts in the installation of the NCLASS code that is now coupled with JETTO code. The authors are also grateful to Emmanuel Joffrin and Marc Beurskens for many fruitful discussions. This work has been conducted under the European Fusion Development Agreement within Task Force S2 and H.

## References

- [1] Levinton F M *et al* 1995 *Phys. Rev. Lett.* **75** 4417
- [2] Strait E J *et al* 1995 *Phys. Rev. Lett.* **75** 4421
- [3] Koide Y *et al* 1998 *Plasma Phys. Control. Fusion* **40** 641
- [4] Wolf R C *et al* 2000 *Phys. Plasmas* **7** 1839
- [5] Turnbull A D, Taylor T S, Lin-Liu Y R and St. John H 1995 *Phys. Rev. Lett.* **75** 718
- [6] Staebler G M *et al* 1998 *Plasma Phys. Control. Fusion* **40** 569
- [7] Kessel C, Manickam J, Rewoldt G and Tang W M *et al* 1994 *Phys. Rev. Lett.* **72** 1212
- [8] Diamond P H *et al* 1997 *Phys. Rev. Lett.* **78** 1472
- [9] Shaing K C, Aydemir A Y, Houlberg W A and Zarnstorff M C 1998 *Phys. Rev. Lett.* **80** 5353
- [10] Beer M A *et al* 1997 *Phys. Plasmas* **4** 1792
- [11] Dorland W, Jenko F, Kotschenreuther M and Rogers B N 2000 *Phys. Rev. Lett.* **85** 5579
- [12] Doyle E J *et al* 2000 *Proc. 18th IAEA Fusion Energy Conference (Sorrento, Italy, 4–10 October, 2000)* IAEA-CN-77/EX6/2
- [13] Tala T J J *et al* 2001 *Plasma Phys. Control. Fusion* **43** 506
- [14] Greenfield C M *et al* 1999 *Nucl. Fusion* **39** 1723
- [15] Greenfield C M *et al* 2000 *Phys. Plasmas* **7** 1959
- [16] Prater R *et al* 2000 *Proc. 18th IAEA Fusion Energy Conference (Sorrento, Italy, 4–10 October, 2000)* IAEA-CN-77/EX8/1
- [17] Fujita T *et al* 2000 *Proc. 18th IAEA Fusion Energy Conference (Sorrento, Italy, 4–10 October, 2000)* IAEA-CN-77/EX4/1
- [18] Challis C D *et al* 2002 *Plasma Phys. Control. Fusion* submitted
- [19] Dumont R, Giruzzi G and Barbato E 2000 *Phys. Plasmas* **7** 4972
- [20] Lopez-Bruna D, Carreras B A and Newman D E 2000 *Nucl. Fusion* **40** 1825
- [21] Genacchi G and Taroni A 1988 JETTO: A free boundary plasma transport code (basic version), *Rapporto ENEA RT/TIB 1988(5)*

- [22] Hirshman S P, Hawryluk R J and Birge B 1977 *Report* PPPL-1326
- [23] Tala T J J *et al* 2000 *Nucl. Fusion* **40** 1635
- [24] Parail V V *et al* 1999 *Nucl. Fusion* **39** 429
- [25] Erba M *et al* 1997 *Plasma Phys. Control. Fusion* **39** 261
- [26] Erba M *et al* 1996 Validation of a new mixed Bohm/gyro-Bohm transport model on discharges of ITER date-base *Report* JET-R(96)07, JET Joint Undertaking
- [27] Hinton F L and Hazeltine R D 1976 *Rev. Mod. Phys.* **48** 239
- [28] Ohkawa T 1978 *Phys. Lett. A* **67** 35
- [29] Jenko F *et al* 2000 *Phys. Plasmas* **7** 1904
- [30] Hahm T S and Burrell K H 1995 *Phys. Plasmas* **2** 1648
- [31] Challis C D *et al* 2001 *Plasma Phys. Control. Fusion* **43** 861
- [32] Joffrin E *et al* 2001 MHD internal transport barrier triggering in low positive shear scenario in JET *Nucl. Fusion* submitted
- [33] de Esch H P L, Stork D and Weisen H 1990 *Proc. 17th European Physical Society Conf. on Controlled Fusion and Plasma Physics (Amsterdam, The Netherlands, 25–29 June, 1990)* (ECA vol 14B) p 90
- [34] Lao L *et al* 1985 *Nucl. Fusion* **25** 1611
- [35] Esterkin A R and Piliya A D 1996 *Nucl. Fusion* **36** 1501
- [36] Heikkinen J A *et al* 1999 *Plasma Phys. Control. Fusion* **41** 1231
- [37] Challis C D *et al* 1989 *Nucl. Fusion* **29** 563
- [38] Nowak S, Lazzaro E and Ramponi G 1996 *Phys. Plasmas* **3** 4140
- [39] Eriksson L-G, Hellsten T and Willen U 1993 *Nucl. Fusion* **33** 1037
- [40] Carlsson J, Eriksson L-G and Hellsten T 1994 *Proc. Joint Varenna–Lausanne Workshop ‘Theory of Fusion Plasmas’* (Bologna: Editrice Compositorei) p 351
- [41] Hawkes N C *et al* 2002 *Plasma Phys. Control. Fusion* submitted
- [42] Hawkes N C *et al* 2001 Observation of zero current density in the core of JET discharges with lower hybrid heating and current drive *Phys. Rev. Lett.* submitted
- [43] Ward D J 1994 *Plasma Phys. Control. Fusion* **36** 673
- [44] Houlberg W A *et al* 1997 *Phys. Plasmas* **4** 3231
- [45] Joffrin E *et al* 2002 *Plasma Phys. Control. Fusion* submitted
- [46] Litaudon X *et al* 2002 *Plasma Phys. Control. Fusion* submitted
- [47] Hogeweij G M D *et al* 2002 *Plasma Phys. Control. Fusion* submitted
- [48] Mailloux J *et al* 2001 to appear in *Proc. 28th European Physical Society Conf. on Controlled Fusion and Plasma Physics (Madeira, Portugal, 18–22 June, 2001)*
- [49] Dux R *et al* 2002 *Plasma Phys. Control. Fusion* submitted
- [50] Hender T *et al* 2002 *Plasma Phys. Control. Fusion* submitted
- [51] In Y *et al* 2000 *Nucl. Fusion* **40** 1463